COBEM 2023 27TH INTERNATIONAL CONGRESS OF MECHANICAL ENGENEERING

ABCM Brazilian Society of Mechanical Sciences and Engineering
27th ABCM International Congress of Mechanical Engineering
December 04-08, 2023, Florianópolis-SC, Brazil

COBEM 2023-1274
EFFICIENCE OF SOLAR PHOTOVOLTAIC MODULES SUBMERGED AND PLACED ON THE WATER SURFACE: evaluation using thermal models.

Humberto Faria Rezende
Instituto Federal de Minas Gerais
rezende.humberto23@gmail.com
Ricardo Carpio Carrasco
Instituto Federal de Minas Gerais
ricardo.carpio@ifmg.edu.br
Francisco de Sousa Júnior
Instituto Federal de Minas Gerais
francisco.sousa@ifmg.edu.br
Vinícius Silva Nunes
Instituto Federal de Minas Gerais
viniciusnunesengmec@gmail.com

Abstract. *This study examines the impact of installing photovoltaic solar panels on water or near its surface. We theoretically calculated the potential increase in energy generation efficiency of these panels, taking into account the efficiency reduction caused by temperature rise. Heat transfer calculations, solar incidence angle, and light absorption by the solar cells were performed. The Python programming language was used to perform the calculations and determine heat exchange, equipment temperature, and energy generation. It was observed that panels installed in water showed a significant temperature reduction, resulting in a 6.43% increase in energy generation on clear sky days and a 9.70% increase when submerged 4 cm below the water surface compared to conventional panels. Based on the calculations conducted, it can be concluded that installing solar panels on or near water is beneficial, leading to a substantial increase in output power under high solar irradiation conditions.*
Keywords: *Photovoltaic, Thermal exchange, Thermal models, Energy generation.*

1. INTRODUCTION

In 2020, the Brazilian electrical grid achieved 84.8% of generation from renewable sources, primarily through the use of hydroelectric power plants.(EPE, 2022). However, there is a forecasted increase in electricity consumption in the country, and the limited development of the national energy supply could potentially lead to a new crisis.(Martins and Pereira, 2011).

In addition to the high annual solar radiation incidence in Brazil, the seasonal and interannual variations are low due to the fact that a large part of the national territory is located in the tropical region. This makes the use of solar technology economically viable throughout the country, even considering the specific conditions of each region. As a result, Brazil has one of the highest potentials for solar energy generation to be explored (Martins and Pereira, 2011).

Photovoltaic generation based on crystalline silicon photovoltaic cells is a well-established technology, with installations around the world producing clean electrical energy. However, its performance is strongly affected by the increase in equipment temperature, especially during periods of high solar radiation incidence (Bevilacqua *et al.*, 2021).

The installation of panels near the water surface has proven to be advantageous, as it offers beneficial effects such as a significant reduction in equipment temperature, reduced reflection due to the water's refractive index, and lower accumulation of impurities. This allows for higher energy generation compared to conventional panels (Lanzafame *et al.*, 2009).

2. METHODOLOGY

For the development of the study, three assembly configurations of the photovoltaic modules were utilized: the conventional method, where the modules are mounted on the ground; on a surface above water; and submerged in water at a depth of 4 cm, as shown in the figure1 . The objective was to conduct a study on the thermal exchange in the photovoltaic solar panel, considering solar radiation.

It is crucial to understand the fundamental difference between radiation and irradiation. Radiation involves the movement of energy particles, while irradiation pertains to the impact of radiation on an object. This implies that the term

"irradiation" encompasses the process of interaction between the two. Consequently, something begins to emit energy as soon as it comes into contact with radiation.

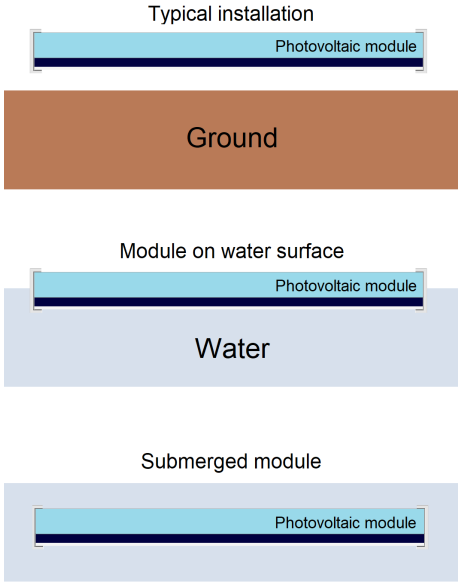

Figure 1. Studied installation conditions.
Source: Own authors

The assumption of a depth of 4 cm was based on the study of (Lanzafame *et al.*, 2009), the consideration of a depth of 4 cm was based on a study that found a significant increase in energy generation from a solar panel when installed at a depth of 4 cm. This is due to the more effective cooling provided by the water, which reduced the effects of efficiency loss in the panel due to temperature rise.

2.1 Identification of energy exchange components in the panel

Due to the variation in electrical energy generated as a function of the temperature of the photovoltaic solar panel, it is necessary to understand the inputs and outputs of energy. This includes the solar radiation incidence, reflected and absorbed by the materials, as well as the electrical energy generated by the equipment and the dissipation of heat to the environment.

In order to illustrate and promote the understanding of this process, figure 2 presents a simplification of the energy exchange that occurs within the module, with the lines incident on the cross-sectional view of the panel representing solar light. A portion of the incident light is lost due to the panel structure (*Ge*), That is isolated from the other components. A portion of the light reaches the bottom protection (backsheet), and part of it is lost (*Grb*), While another portion is reflected towards the cell (*Grbc*), contributing to power generation. Some of the light is reflected on the glass surface (*Grv*), while the rest is absorbed by it (*Gav*). The solar light that reaches the cell is partially reflected (*Grc*), while the remaining, a considerably significant portion represented by the thicker line, is absorbed by the silicon in the cell, converted into electrical energy (*P*), and dissipated as heat (*qc*).

In the figure 2 a thermal circuit is presented, illustrating temperatures, emitted heat, and solar radiation. In the circuit, the heat dissipated by the cell *qc* at a temperature *Tc* is partially transferred to the lower surface at a temperature *Tsi* through thermal conduction. At the lower surface, convection and radiation are simultaneously responsible for heat dissipation to the surroundings at a temperature *Ta*. The remaining heat supplied by the cell is conducted to the upper surface at a temperature *Tss* through conduction. In the middle of the glass thickness (with temperature *Tv*), the light absorbed by the material *Gav* and converted into heat is added to the circuit, also conducted to the upper surface. At the upper surface, the heat transfer mechanisms of convection and radiation are responsible for heat dissipation, considering the ambient temperature *Ta* for convection and the equivalent sky temperature *Tsky* for radiation.

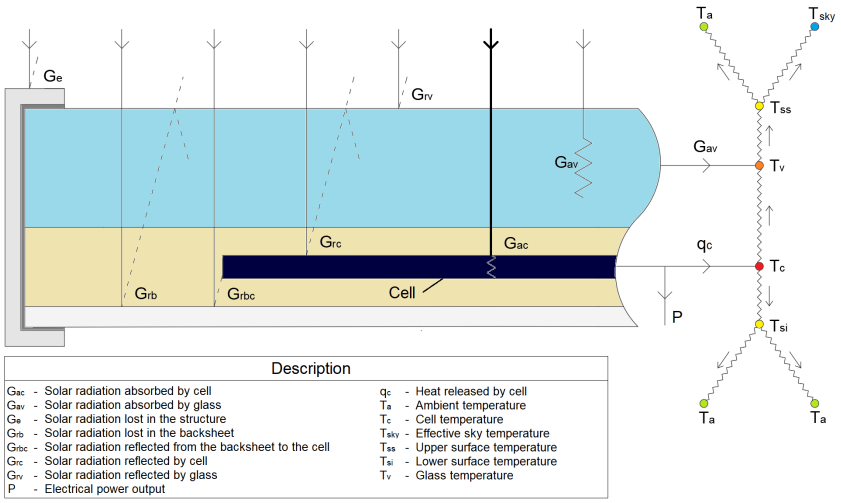

Figure 2. Simplified representation of energy exchange in a solar panel
Source: Own authors

2.2 Calculation of energy production as a function of temperature and solar radiation

To facilitate the calculation of energy production, we rely on the simplifications made by (Luque and Hegedus, 2011), utilize the equipment efficiency (η_{painel}) as a function of its efficiency under reference conditions (η^*_{painel}), where (γ) is the temperature coefficient of the equipment, and the temperature difference between the panel and the reference temperature is assumed as described in the equation 1.

$$\eta_{painel} = \eta^*_{painel} \cdot [1 - \gamma(Tc - 25^oC)], \tag{1}$$

In the case of the submerged panel, the water simultaneously reduces the angle of incidence of sunlight and the reflection on the glass surface. In the studied case, where light passes from air to water and from water to glass, the figure 3 demonstrates that the sum of the reflections occurring during the light's passage through the three materials is still lower than the reflection that occurs at the air/glass interface in conventional panels.

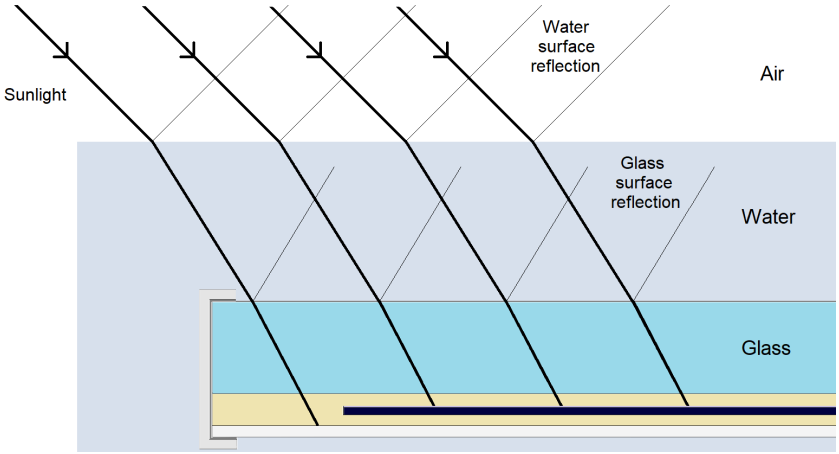

Figure 3. Reflection on the submerged panel.
Source: Own authors

Since we are working with the panel under adverse conditions, which reduces the reflection of light on the upper surface of the solar panel, it is not possible to use the equation 1 presented. To calculate the power generation of the submerged panel, a closed steady-state system was assumed as illustrated in the figure 4, the control volume is highlighted with dashed lines.

Therefore, the energy entering will be equal to the energy leaving. The power generation of the cell was calculated based on the manufacturer's reference conditions for the panel. The efficiency under reference conditions was defined as the ratio of the electrical power generated (W) to the solar radiation received by the cell (*Grbc, Gac, and Grc*).

Based on the cell efficiency under reference conditions, the power generation was calculated based solar radiation reaching the cells, taking into account the temperature coefficient of the equipment determined by the manufacturer.

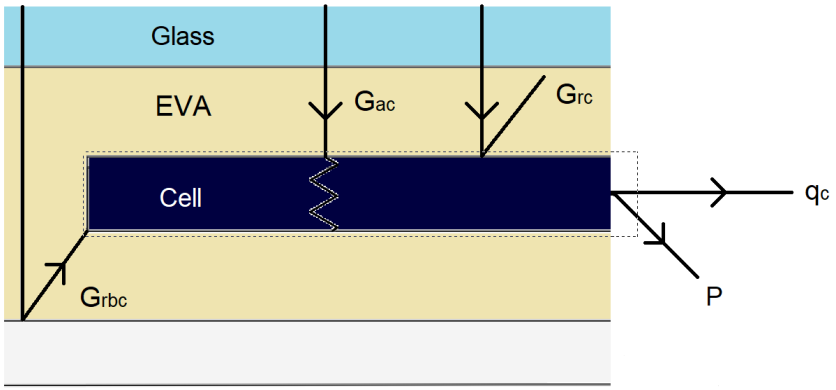

Figure 4. Closed system defined within the cell.
Source: Own authors

2.3 Solar light irradiance intensity and angle of incidence

The intensity of solar radiation is crucial for the design of solar collectors, photovoltaic panels, and solar heating/cooling systems. It is essential to understand the characteristics of solar energy outside the Earth's atmosphere, its intensity, and variations throughout the day and seasons in different locations (Majumdar, 2021).

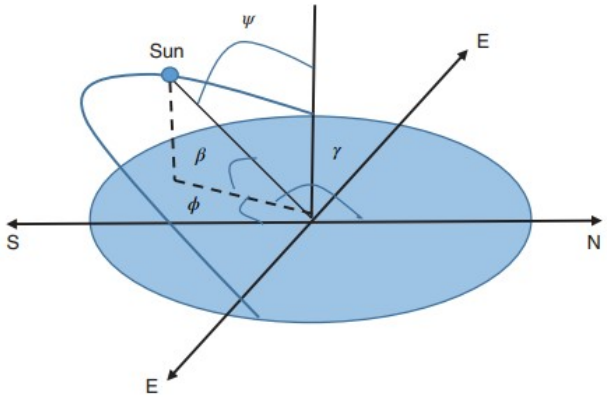

Figure 5. Demonstration of solar angles: Sun's zenith, altitude angle, and azimuth angles.
Source: Adapted from (Majumdar, 2021).

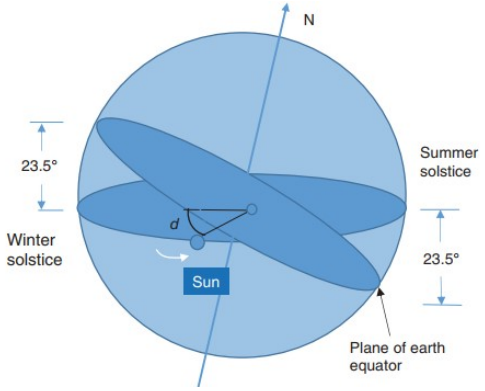

Figure 6. Display Sun's path and declination angle.
Source: Adapted from (Majumdar, 2021).

To illustrate the solar altitude angle and the angle of incidence, we have the figure 5, where (θ) represents the angle of incidence of solar radiation, or zenith angle, which is complementary to the solar altitude or elevation angle (β). The solar altitude angle is defined based on the equation 2. The solar altitude angle is the angle in a vertical plane between the solar radiation and its projection onto the horizontal plane of the observer (Majumdar, 2021).

$$cos(\theta) = sen(\beta) = cos(l) \cdot cos(h) \cdot cos(d) + sen(l) \cdot sen(d) \quad (2)$$

For the equation 2, *l* represents the observer's latitude angle, *h* is the solar hour angle, and *d* is the solar declination angle. The solar declination angle varies annually between -23.45^o e +23.45^o and represents the inclination of the line connecting the center of the Earth to the center of the Sun projected onto the plane of the Earth's equator (Majumdar, 2021). We can obtain the declination angle *d* from the equation 3, where *n* represents the day of the year. (Hodge, 2017).

$$d = 23.45^o \cdot sen[360^o \cdot (284 + n)/365] \tag{3}$$

The solar hour angle *h* is defined in terms of local solar time (*LST*), following the equation 4. The solar hour angle varies from 0° at local solar noon and changes in increments of 15° per hour, with negative values in the morning and positive values in the afternoon (Hodge, 2017).

$$h = (LST - 12:00) \cdot 15^o \tag{4}$$

Local solar time (*LST*) is calculated by considering the observer's longitude (*LCT*) and the correction resulting from the equation of time (*E*), according to the equation 5.

The difference between the observer's meridian and the reference meridian for local time determines (*LCT*), where each 1^o degree of difference represents a 4-minute interval between the times (Majumdar, 2021).

$$LST = LCT + E \tag{5}$$

The equation 6, of time calculates the time correction in minutes. This equation adjusts the local solar time by taking into account the variations in the Earth's rotation speed (Scheffe, 2020).

$$E = 229.2 \cdot (0.000075 + 0.001868 \cdot cos(Bt) - 0.032077 \cdot sen(Bt) - 0.014615 \cdot cos(2Bt) - 0.04089 \cdot sen(2Bt), \tag{6}$$

To obtain the value of Bt, the equation was used 7, *n* represents days of the year (Scheffe, 2020)

$$Bt = (n - 1) \cdot 360/365 \tag{7}$$

Once the solar incidence angle is determined at a given moment, it is possible to calculate the solar irradiation on the surface, taking into account the time of day, day of the year, atmospheric scattering, and other factors. The total solar radiation on the surface consists of direct radiation, diffuse radiation, and reflected radiation. The normal flux of direct solar radiation can be calculated for a clear sky day using the equation 8 (Majumdar, 2021).

$$GND = A^{-B/sen(\beta)} \tag{8}$$

In equatio 8, GND represents the normal direct solar radiation flux in W/m^2. The values of A and B are empirically determined on clear sky days and vary throughout the year due to the distance between the Earth and the Sun and atmospheric conditions. Table1 presents the values presents the typical values of A and B on the twenty-first day of each month (Majumdar, 2021).

Table 1. Average monthly solar radiation outside the atmosphere

Month	**A (w/m²)**	**B**	**C**
January	1230	0.142	0.058
February	12315	0.144	0.06
March	1186	0.156	0.071
April	1136	0.180	0.097
May	1104	0.196	0.121
June	1088	0.205	0.134
July	1085	0.207	0.136
August	1107	0.201	0.122
September	1151	0.177	0.092
October	1192	0.160	0.073
November	1221	0.149	0.063
December	1233	0.142	0.057

Source: Adapted from (Majumdar, 2021).

The direct radiation that reaches the surface can be calculated using Equation 9, where GD represents the direct solar radiation.

$$GD = GND \cdot cos(\theta) \tag{9}$$

The diffuse radiation that reaches a horizontal surface can be defined using the equation 10 (Majumdar, 2021).

$$Gd = C \cdot GND \tag{10}$$

In Equation 10, C represents the ratio between diffuse radiation and direct radiation on a horizontal surface. Table 1 presents the average values of constant C on the twenty-first day of each month. Based on the values of direct and diffuse solar radiation, it is possible to calculate the total radiation.(G) the total radiation that reaches the surface is defined as the sum of direct radiation, diffuse radiation, and reflected radiation. For inclined surfaces or walls, it is also necessary to consider the solar radiation reflected by nearby surfaces(Majumdar, 2021).

$$G = GD + Gd \tag{11}$$

2.4 Code creation Python

Initially, a code was developed using the Jupyter Notebook tool (Kluyver *et al.*, 2016), version 6.3.0, based on the Python programming language (Python Software Foundation, 2021),

version 3.8.8, the calculations described in section 2.3 were implemented in the code in order to streamline the entire process. The values of coefficients A, B, and C from Table 1 were included as well, were interpolated for each day of the year. For the calculations, the latitude and longitude values correspond to the Furnas hydroelectric power plant in Minas Gerais (Google Earth, 2021).

The main parameters required for the heat transfer calculation were obtained from the manufacturer Canadian Solar, from the model of monocrystalline solar panel *CS3W-450MS*, a commercially available model in Brazil with a nominal power of 450 W e 20.4 % efficiency (Canadin Solar, 2019) the table 2 presents the parameters of the selected panel.

Table 2. Solar panel parameters

Parameter	**Value**	**Unit**
Temperature coefficient	-0.35	%/^{0}C
Module length	1.048	m
Module efficiency (STC)	20.4	%
Glass thickness	3.2	mm
Irradiation (NMOT)	800	W/m^2
Irradiation (STC)	1000	W/m^2
Structure width	11	mm
Module width	2.1108	m
Nominal maximum power (NMOT)	336	W
Nominal maximum power (STC)	450	W
Number of cells	144	-
Ambient temperature (NMOT)	20	^{o}C.
Cell temperature under standard test conditions(STC)	25	^{o}C.
Nominal operating temperature of the module (NMOT)	43 $\pm$ 3	^{o}C.
Wind speed	1	m/s

Source: Adapted from (Canadin Solar, 2019).

The manufacturer did not provide some data regarding the internal components of the panel. For the low-iron glass, the thermal conductivity of the material was considered to be 0. 937 W/m.K (Jns Glass & Coatings, 2021). The calculations for conduction within the module were based on the data obtained from (Lee *et al.*, 2008), in the table 3.

Table 3. Thickness and thermal conductivity of the materials.

Material	**Thickness (mm)**	**Thermal conductivity (W /m .K)**
EVA,	0.5	0.23
Anti-reflective coating,	0.1 x 10^{-3}	1.38
Silicon,	0.4	1.48
Backsheet,	0.1	0.36

Source: Adapted from (Lee *et al.*, 2008).

Some assumptions were made, with the refractive indices values used for air and glass being 1 and 1.526, respectively, and the extinction coefficient of the glass having a value of 7 m^{-1} (Majumdar, 2021). It was also considered that the

cell reflects 5.2%, and the bottom protection allows for the recovery of 46% of the light. The emissivity of the glass was assumed to be 0.925, and the emissivity of the ground was taken as 0.95 (Çengel, 2009), The emissivity of water was assumed to be 0.96 (Majumdar, 2021). The emissivity of the backsheet was assumed to be 0.90 (Zhou *et al.*, 2015).

For convection heat transfer calculations, the values were obtained through the implementation of the CoolProp tool (Bell *et al.*, 2014), version 6.4.1, for the Python language, with the values extracted at atmospheric pressure and based on the film temperature. In calculations involving heat transfer inside the panel, an iterative process was used. The calculation process is described in Figure 7:

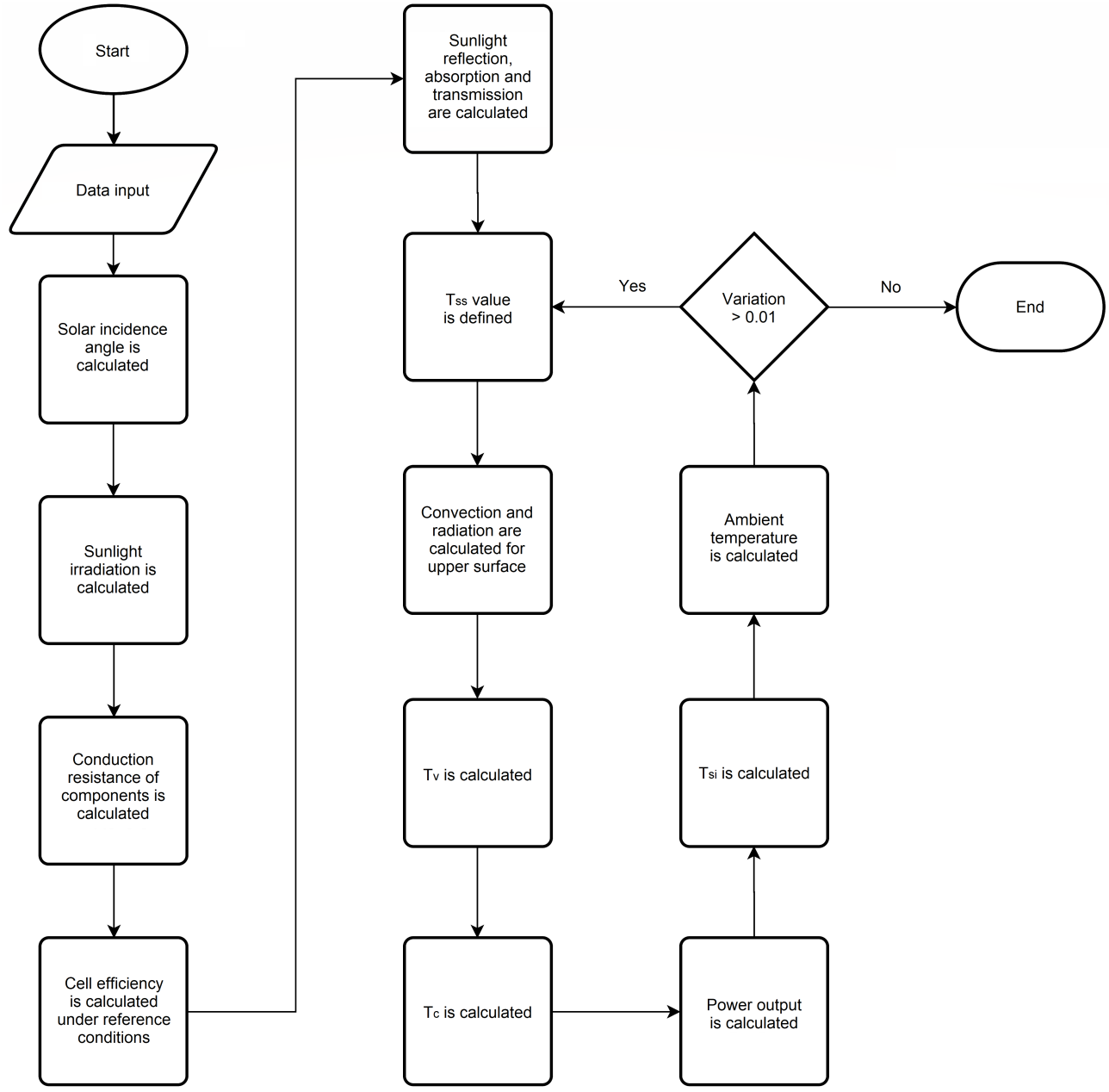

Figure 7. Flowchart of the code execution Python
Source: Own authors

3. RESULT

3.1 Solar radiation and angle of incidence

The figure 8 graphically represents the angle of incidence is represented in red on the summer solstice, when there is a higher incidence of sunlight, and in blue on the winter solstice, when there is a lower incidence of sunlight. It should be noted that the values were calculated for clear sky days. On the summer solstice, a maximum irradiation value of 1129W/m^2, while on the winter solstice, the maximum calculated value was 696 W/m^2.

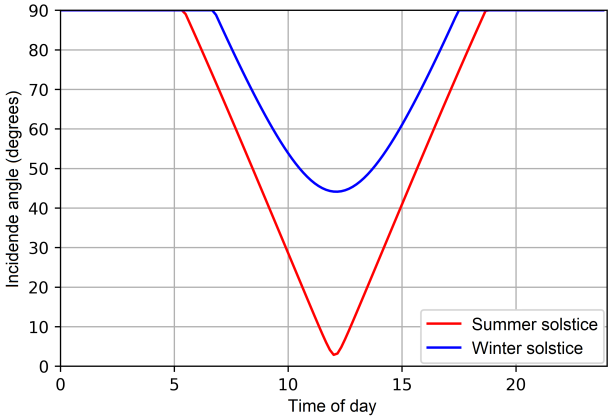

Figure 8. Angle of incidence of sunlight on the solstices
Source: Own authors

Figure 9 shows the temperature of the studied panels as a function of solar irradiation, considering an angle of incidence of zero degrees9.

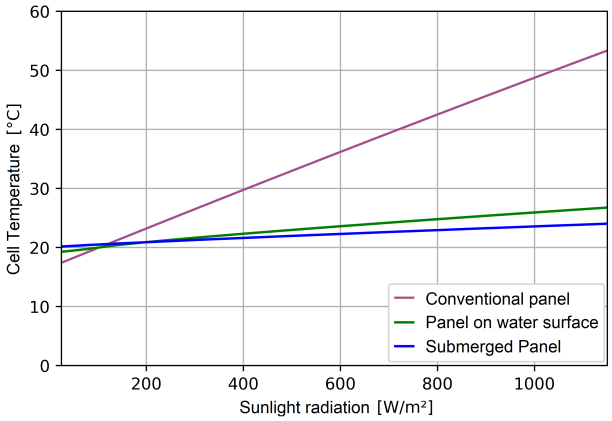

Figure 9. Temperature of the panels as a function of sunlight irradiation
Source: Own authors

The temperature of the panels in contact with water differs significantly from the temperature of the conventional panel as the irradiation increases, due to improved heat dissipation. figure 10 illustrates the power generated by the panels as a function of irradiation, considering an incidence angle of zero degrees.

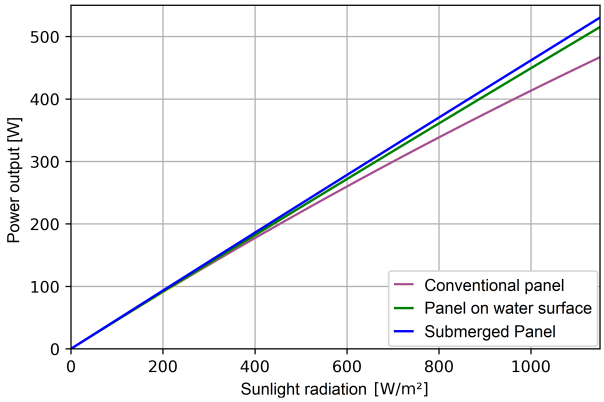

Figure 10. Power of the panels as a function of solar irradiation
Source: Own authors

With an angle of incidence of zero degrees, the reflection of light at the transition from air to glass is 4.34% reduces to 2.47% with the water layer. With an angle of incidence of 45 degrees, the reflection decreases from 5.39% in the conventional panel to 3.26% in the submerged panel. Figure 11 presents the power generated by the panels throughout

the day during the summer and winter solstices.

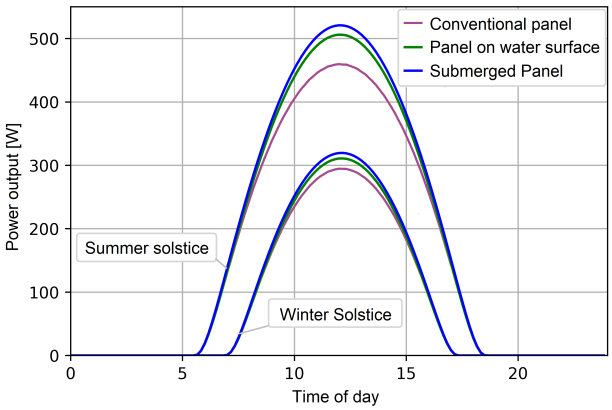

Figure 11. Power of the panels at the solstices
Source: Own authors

During the summer, the panels over water and submerged generated, respectively, 7.56% and 10.86% more energy than the conventional panel. In the winter, the panel over water produced 4.08% more energy, while the submerged panel obtained 7.44% more. Throughout the year, on average, the panels over water and submerged generated 6.43% and 9.70% more energy compared to the conventional panel.

4. CONCLUSIONS

The thermal analysis of the solar panels over water and submerged revealed a significant increase in energy generation compared to conventional panels. The main benefit observed was the significant reduction in panel temperature under high solar irradiation, resulting in lower losses caused by the temperature coefficient of silicon. Additionally, the submerged panel benefited from the reduction in solar light reflection due to the presence of water between the air and the glass surface. According to the calculations, installing the panel over water results in an average annual energy production increase of 6.43% compared to the conventional panel, while installing the panel submerged near the water surface provides a 9.70% increase compared to the conventional panel.

5. REFERENCES

Bell, I.H., Wronski, J., Quoilin, S. and Lemort, V., 2014. "Pure and pseudo-pure fluid thermophysical property evaluation and the open-source thermophysical property library coolprop". *Industrial & Engineering Chemistry Research*, Vol. 53, No. 6, pp. 2498–2508. doi:10.1021/ie4033999. URL `http://pubs.acs.org/doi/abs/10.1021/ie4033999`.

Bevilacqua, P., Perrella, S., Cirone, D., Bruno, R. and Arcuri, N., 2021. "Efficiency improvement of photovoltaic modules via back surface cooling". *Energies*, Vol. 14, No. 4, p. 895. URL `https://www.mdpi.com/1996-1073/14/4/895`.

Canadin Solar, 2019. "Módulo perc de alta potência de células duplas (poly e mono)". URL `https://www.csisolar.com/br/hiku/`.

Çengel, Y.A., 2009. *Transferência de calor e massa: uma abordagem prática*. McGraw-Hill, São Paulo, 3rd edition.

EPE, 2022. "National energy balance 2022, final report (in portuguese)". Empresa de Pesquisa Energética EPE, Rio de Janeiro, epe.gov.br/sites-pt/publicacoes-dados-abertos/publicacoes/PublicacoesArquivos/publicacao-675/topico-638/BEN2022.pdf. Accessed 02 May 2023.

Google Earth, 2021. "Coordenadas referentes à usina hidrelétrica de furnas, minas gerais, brasil". URL `https://earth.google.com/web/`.

Hodge, B.K., 2017. *Alternative Energy Systems and Applications*. Wiley, Hoboken, NJ, EUA, 2nd edition.

Jns Glass & Coatings, 2021. "Low iron glass - ultra clear, starphire, optiwhite". URL `https://jnsglass.com/low-iron-glass/`.

Kluyver, T. *et al.*, 2016. "Jupyter notebooks – a publishing format for reproducible computational workflows". In F. Loizides and B. Schmidt, eds., *Positioning and Power in Academic Publishing: Players, Agents and Agendas*. IOS Press, pp. 87 – 90. URL `https://ebooks.iospress.nl/publication/42900`.

Lanzafame, R., Nachtmann, S., Rosa-Clot, M., Rosa-Clot, P. *et al.*, 2009. "Field experience with performances evaluation of a single-crystalline photovoltaic panel in an underwater environment". *IEEE Transactions on Industrial Electronics*, Vol. 57, No. 7, pp. 2492–2498.

Lee, B., Liu, J., Sun, B., Shen, C. and Dai, G., 2008. "Thermally conductive and electrically insulating eva compos-

ite encapsulants for solar photovoltaic (pv) cell". *eXPRESS Polymer Letters*, Vol. 2, No. 5, pp. 357–363. URL http://www.expresspolymlett.com/articles/EPL-0000613$_a rticle.pdf$.

Luque, A. and Hegedus, S., 2011. *Handbook of Photovoltaic Science and Engineering*. Wiley, 2nd edition.

Majumdar, P., 2021. *Design of Thermal Energy Systems*. Wiley, Hoboken, NJ, EUA, 1st edition.

Martins, F.R. and Pereira, E.B., 2011. "Enhancing information for solar and wind energy technology deployment in brazil". *Energy Policy*, Vol. 39, No. 7, pp. 4378–4390. URL https://l1nq.com/Qh5zb.

Python Software Foundation, 2021. "Python". URL https://www.python.org/.

Scheffe, J., 2020. "Solar time and solar time python calculator". *University of Florida*. URL https://encr.pw/Vt2Al.

Zhou, J., Yi, Q., Wang, Y. and Ye, Z., 2015. "Temperature distribution of photovoltaic module based on finite element simulation". *Solar Energy*, Vol. 111, pp. 97–103.

6. RESPONSIBILITY NOTICE

The authors are solely responsible for the printed material included in this paper.